11th World Congress on Computational Mechanics (WCCM XI)
5th European Conference on Computational Mechanics (ECCM V)
6th European Conference on Computational Fluid Dynamics (ECFD VI)
E. Oñate, J. Oliver and A. Huerta (Eds)

NUMERICAL ISSUES IN HIGHER-ORDER ACCURATE SIMULATIONS OF FLOWS WITH VORTEX CAVITATION

Faraz Khatami*, Edwin T. A. van der Weide* and Harry W. M. Hoeijmakers*

* Mechanical Engineering Department, University of Twente
P.O. box 217, 7500 AE Enschede, The Netherlands
e-mail: f.khatami@utwente.nl, web page: http://www.utwente.nl/ctw/ts/

Key words: Cavitation, WENO, Positivity-preserving, Vortex dynamics

Abstract. *This paper, investigates the feasibility of performing a robust numerical simulation of the dynamics of vortex cavitation. An equilibrium cavitation model is employed, which assumes local thermodynamic and mechanical equilibrium in the two-phase flow region. Furthermore, the phase transition does not depend on empirical constants in this model. The computational method assumes a compressible flow together with appropriate thermodynamic equations of state i.e. Tait's equation for the liquid phase, a perfect gas for the vapor phase, and an equilibrium model for the mixture phase. The unsteady compressible Euler equations are employed using a cell-centered structured multi-block finite volume scheme. The viscous terms are not taken into account, because the numerical issues encountered are typically caused by (the discretization of) the inviscid equations. The 3D vortex cavitation simulations using a MUSCL scheme on an Arndt's elliptic hydrofoil are presented. The results show that the common MUSCL schemes are not well-suited for such complex simulations. For an accurate representation of the cavitating flow, the higher-order accurate Weighted Essentially Non-Oscillatory (WENO)schemes are considered. In order to avoid negative density and/or internal energy, the scheme must fulfill the positivity-preserving property. The existing positivity-preserving approaches use limiter functions to preserve the monotonicity of the solution near the discontinuities. It is well-known that the limiter functions introduce considerable amount of artificial dissipation, which is highly undesirable in vortex cavitation simulations. We propose a non-limiting (no slope/flux limiters) positivity-preserving strategy for WENO schemes, which is rather simple and computationally low-cost. Some 1D test case simulations with or without cavitation are presented to assess the developed positivity-preserving WENO aproach.*

1 INTRODUCTION

Cavitation is an unsteady process which involves appearance and disappearance of vapor cavities in a liquid. Vapor cavities appear in regions where the liquid pressure drops

below the saturation pressure and afterwards disappear in regions with higher pressure. There are many applications involving cavitating flows, some examples are in technical applications such as pumps, turbines, ship propellers, fuel injection systems, bearings, and in medical sciences such as lithotripsy treatment and the flow through artificial heart valves. The appearance and disappearance of vapor regions of cavitating flows in hydraulic systems may cause a number of problems. These include vibration and noise, surface erosion in the case of developed cavitation, and deteriorating the performance of the system such as lift reduction and increase in drag of a foil and loss of turbomachinary efficiency. However, besides the harmful effects, cavitation is used in some industrial processes to produce high pressure peaks and apply it for cleaning of surfaces, dispersion of particles in a liquid, production of emulsions etc. Hence, to be able to control the effects of cavitation, it is essential to understand the driving mechanisms of this phenomenon.

The aim of this paper is to investigate the performance of the different finite volume-based discretization schemes for simulations of the dynamics of vortex cavitation. Due to the presence of discontinuities between the different phases of the cavitating flow, a monotonic reconstruction scheme is necessary in such simulations. It will be shown that the Monotone Upstream-centered Schemes for Conservation Laws (MUSCL) [5] family of reconstruction schemes are not well-suited for such simulations. To remedy this problem, a more sophisicated approach based on the higher-order Weighted Essentially Non-Oscillatory (WENO) [6, 7] reconstruction schemes are considered. Although the WENO schemes have proven their robustness in many applications, it is observed that the WENO-based simulations for the cavitating flows fail near the large discontinuities between the different phases. This is due to presence of very small numerical oscillations near the discontinuities in WENO reconstruction schemes. These oscillations can result in negative values of density and/or internal energy which cause the simulations to crash. To overcome this problem, a positivity-preserving method must be used. The existing positivity-preserving approaches [8, 9] use limiter functions in order to preserve the monotonicity of the solution near the discontinuities. It is well-known that limiter functions introduce extra artificial dissipation in simulations, which is highly undesirable in vortex cavitation simulations. We develop a non-limiting (no slope/flux limiters) positivity-preserving strategy for WENO scheme, which is rather simple and computationally low-cost. In order to assess the method, first the Sod shock tube test case [11] is considered and the results based on the developed positivity preserving WENO simulations are compared to the ones obtained using the characteristic-wise WENO and MUSCL schemes. Next, the method is applied to a 1D cavitating expanding waves test case [12], noting that the inspected non-positivity preserving WENO schemes failed in these simulations. The results using the positivity-preserving WENO approach are compared to the results of the MUSCL approach.

This paper is organized as follows. In section 2, the physical model is described including the thermodynamic closure relations. Section 3 describes the discretization schemes, followed by results in section 4.

2 PHYSICAL MODELING

In order to perform numerical simulations of the flows with vortex cavitation, some assumptions are used. To be able to capture the shock waves, the flow is considered compressible. Based on the cavitation equilibrium model [1] which is used in this study, the two-phase flow regime is assumed to be a homogeneous mixture of liquid and vapor. Furthermore relative velocities between the liquid and vapor parts are neglected, and local pressure and temperature equilibrium are assumed. In other words, the two-phase flow is in mechanical and thermodynamic equilibrium.

Based on these assumptions, appropriate thermodynamic equations need to be introduced to cover all the possible states. The equations of state must preserve the hyperbolic nature of the resulting system of equations so that the pressure waves in the fluid can be represented. When the viscous terms are neglected, the governing equations of motion for the model described above are the Euler equations which in integral conservation form are given by

$$\frac{\partial}{\partial t}\iiint_{\Omega} \mathbf{U}\,\mathrm{d}\Omega + \iint_{\Gamma=\partial\Omega} \vec{\mathbf{F}}\left(\mathbf{U}\right).\mathbf{n}\,\mathrm{d}\Gamma = 0. \tag{1}$$

Here it is assumed that Ω is a bounded polygon domain in $\mathbb{R}^3$ with boundary $\partial\Omega$, the vector $\mathbf{U}$ denotes the vector of conservative variables, that is $\mathbf{U} = [\rho, \rho u, \rho v, \rho w, \rho E]$ and $\vec{\mathbf{F}}\left(\mathbf{U}\right)\cdot\mathbf{n}$ is the normal component of the inviscid flux vector in Cartesian coordinates

$$\vec{\mathbf{F}}\left(\mathbf{U}\right).\mathbf{n} = \begin{bmatrix} \rho\hat{u} \\ \rho\hat{u}u + pn_x \\ \rho\hat{u}v + pn_y \\ \rho\hat{u}w + pn_z \\ \rho\hat{u}H \end{bmatrix}, \tag{2}$$

where $\hat{u}$ is the velocity normal to the surface Γ that is $\hat{u} = \mathbf{u}\cdot\mathbf{n}$. Furthermore H denotes the total enthalpy

$$H = E + \frac{p}{\rho} = h + \frac{1}{2}\mathbf{u}.\mathbf{u}, \tag{3}$$

where E and h are the total energy and specific static enthalpy, $h = e + p/\rho$, respectively. E is defined as

$$E = e + \frac{1}{2}\mathbf{u}.\mathbf{u}, \tag{4}$$

where e denotes the specific internal energy.

The unknowns for the system of equations are $\{\rho, u, v, w, e, p, T\}$, To close the system of equations two additional equations are needed, which are given by the thermodynamics,

namely $p = p(\rho, T)$ and $h = h(p, T)$. These relations must be known for the liquid, vapor, and mixture phases. In the following equations of state are given. The expressions for liquid, vapor, and saturation densities are denoted by subscripts l, v, and sat, respectively. An acoustic speed of sound formula is used in liquid and vapor phases as

$$c^2 = \left(\frac{\partial p}{\partial \rho}\right)_e + \frac{p}{\rho^2}\left(\frac{\partial p}{\partial e}\right)_\rho. \tag{5}$$

In the mixture phase, instead of the acoustic speed of sound the simplified Wallis formula for speed of sound [13] is used as

$$\frac{1}{\rho c^2} = \frac{\alpha}{\rho_{v,sat}(T)\, c_v^2} + \frac{1-\alpha}{\rho_{l,sat}(T)\, c_l^2}. \tag{6}$$

This is to increase the stability of the numerical simulations [14].

2.1 Liquid phase

Following the studies which use the cavitation equilibrium model [1, 3] A modified Tait equation of state is used which describes the liquid pressure in terms of density and temperature

$$p_l(\rho_l, T_l) = K_0\left[\left(\frac{\rho_l}{\rho_{l,sat}(T_l)}\right)^N - 1\right] + p_{sat}(T_l), \tag{7}$$

where for water $K_0 = 3.3 \times 10^8\, Pa$ and $N = 7.15$ are constants. An approximate caloric equation of state, given by

$$e_l(\rho_l, T_l) = e_l(T_l) = C_{vl}(T_l - T_0) + e_{l0}, \tag{8}$$

is adopted which provides a good approximation [2]. The constants in the above equation with their corresponding values for water are defined as: $C_{vl} = 4180\,\mathrm{J\,kg^{-1}\,K^{-1}}$, the specific heat at constant volume, $T_0 = 273.15\,\mathrm{K}$ a reference temperature, and $e_{l0} = 617.0\,\mathrm{J\,kg^{-1}}$ a reference internal energy.

2.2 Vapor phase

The equations of state for the vapor phase are based on a calorically perfect gas model. Therefore the corresponding equation for the pressure is

$$p_v(\rho_v, T_v) = \rho_v R T_v \tag{9}$$

and the caloric equation of state can be expressed as

$$e_v(T_v) = C_{vv}(T_v - T_0) + L_v(T_0) + e_{l0}, \tag{10}$$

where the constants with their corresponding values for water vapor are defined as: $L_v(T_0) = 2.3753 \times 10^6\,\mathrm{J\,kg^{-1}}$ the latent heat of vaporization, $T_0 = 273.15\,\mathrm{K}$ the reference temperature, and $C_{vv} = 1410.8\,\mathrm{J\,kg^{-1}\,K^{-1}}$ the specific heat at constant volume.

2.3 Mixture phase

For the mixture phase it is assumed that the liquid and vapor phases are in mechanical and thermodynamic equilibrium. The equation of state for pressure is considered by taking the mixture pressure equal to the saturation pressure:

$$p_l = p_v = p_{sat}\left(T\right). \tag{11}$$

The mixture density can be written as

$$\rho = \alpha\rho_{v,sat}\left(T\right) + \left(1-\alpha\right)\rho_{l,sat}\left(T\right), \tag{12}$$

and the caloric equation of state for the mixture is defined by

$$\rho e = \alpha\rho_{v,sat}\left(T\right)e_v(T) + \left(1-\alpha\right)\rho_{l,sat}e_l\left(T\right) \tag{13}$$

where α is the void fraction of the vapor. The saturation parameters are functions of temperature and are obtained via the following curve fits [15].

$$\ln\left(\frac{p_{sat}\left(T\right)}{p_c}\right) = \frac{T_c}{T}\sum_{i=1}^{7} a_i\theta^{\hat{a}_i}, \tag{14}$$

$$\frac{\rho_{l,sat}\left(T\right)}{\rho_c} = \sum_{i=1}^{7} b_i\theta^{\hat{b}_i}, \tag{15}$$

$$\ln\left(\frac{\rho_{v,sat}\left(T\right)}{\rho_c}\right) = \sum_{i=1}^{7} c_i\theta^{\hat{c}_i}, \tag{16}$$

where $a_i, \hat{a}_i, b_i, \hat{b}_i, c_i, \hat{c}_i$ are constants (see [15] for the actual values). These functions are valid for ranges of temperature $T_r \leq T \leq T_c$, where T_r, and T_c are the triple point and critical point temperatures, respectively. The values of the constants used in the above expressions are $T_c = 647.16\,\mathrm{K},\ p_c = 22.12\times10^6\,\mathrm{Pa},\ \rho_c = 322.0\,\mathrm{kg\ m^{-3}},\ T_r = 273.15\,\mathrm{K}$.

Following [4], the precomputed multi-phase thermodynamic tables approach is employed for the presented equations. Furthermore, the Phase-Oriented Interpolations in Transition Cells (POITC) look-up procedure is used for data interpolations from these tables.

3 DISCRETIZATION METHOD

The governing equations (equation (1)) are solved using a cell-centered finite volume approach on multiblock structured grids. Dividing the physical domain in a set of non-overlapping non-deforming volumes V_i with boundary ∂V_i, and replacing the inter-cell flux by a numerical flux $\mathbf{H}$ which is assumed to be constant over face S_{ij}, the discretized form of the equations for each volume at time level t^n can be written as

$$\frac{\partial\bar{\mathbf{U}}_i}{\partial t} = -\Re_i, \tag{17}$$

where

$$\bar{\mathbf{U}}_i = \frac{1}{|V_i|} \iiint_{V_i} \mathbf{U} \, \mathrm{d}\Omega \tag{18}$$

and $\Re_i$ is the spatial residual

$$\Re_i = \frac{1}{|V_i|} \sum_{j=1}^{N_{S,i}} \mathbf{H} \left(\mathbf{U}_L, \mathbf{U}_R, \mathbf{n_{ij}} \right) |S_{ij}| \, . \tag{19}$$

$\mathbf{U}_L$ and $\mathbf{U}_R$ are the variables on left and right sides of the volume's face and are determined via the reconstruction technique.

In this paper both the MUSCL reconstruction schemes [5], and the Weighted Essentially Non-Oscillatory (WENO) reconstruction schemes [6, 7] are considered (see section 3.1). For the MUSCL scheme a MinMod limiter is used to guarantee the monotonicity property. Additionally, the actual reconstruction variables are density, three components of velocity and internal energy, i.e. $\{\rho, u, v, w, e\}$. This turned out to be a more stable reconstruction than using the conservative variables $\{\rho, \rho u, \rho v, \rho w, \rho E\}$, because for the latter it cannot be guaranteed that the internal energy is interpolated monotonically, which is crucial for the stability of the method.

Using the reconstructed variables, the fluxes are computed by an approximate Riemann solver. The solution based on the classical Riemann solvers for cavitation becomes much too dissipative in low-Mach number flow regimes. To remedy this problem, a hybrid HLLC/AUSM flux scheme [1] is used. In this approach, the mass flux is calculated based on the HLLC scheme [16], and the pressure flux is determined based on the AUSM scheme [17]. For the numerical flux scheme $\mathbf{H}$ in equation (19), we use the hybrid HLLC/AUSM scheme. Finally, for the time discretization, a third order accurate three-stage TVD Runge-Kutta method [10] is used.

3.1 Weighted Essentially Non-Oscillatory (WENO) scheme

WENO schemes perform polynomial reconstructions in an adaptive stencil manner such that using the local smoothness indicators of the solution, the smoothest solution is automatically chosen to achieve a high-order accurate solution with no oscillations (or very small) near the discontinuities.

3.1.1 A positivity-preserving WENO strategy

In order to describe the developed positivity-preserving strategy, we start by writing the 1D Euler eqution in quasi-linear form

$$\frac{\partial q}{\partial t} + A_q \frac{\partial q}{\partial x} = 0, \tag{20}$$

where $q = (\rho, \rho u, \rho E)$ are the conservative variables, and A_q is the flux jacobian matrix with respect to the variables q.

In order to preserve the positivity, the properties of the logarithmic mapping and inverse exponential mappings are used. Additionally, this approach works effectively only when a characteristic-wise reconstruction of a carefully chosen set of variables is performed. For the reconstruction variables, we choose a set of semi-logarithmic semi-conservative variables $Q = (\ln(\rho), u, \ln(\rho E))$. Based on the variables Q, a transformation of the equations 20 yields

$$\frac{\partial Q}{\partial t} + A_Q \frac{\partial Q}{\partial x} = 0, \tag{21}$$

where A_Q is the transformed flux jacobian based on the variables Q. In order to perform a characteristic-wise reconstruction of the variables Q, a decoupling of the system of equations (21) is performed based on the transformed variables $w = R_Q^{-1} Q$, with R_Q the matrix of the right eigenvectors of A_Q. The resulting scalar equations are

$$\frac{\partial w}{\partial t} + \Lambda \frac{\partial w}{\partial x} = 0, \tag{22}$$

where Λ is the diagonal matrix of the eigenvalues. Then, the WENO scheme is used to obtain $w_{i+1/2}$ face values. Through a reverse transformation, the semi-logarithmic semi-conservative face variables $Q_{i+1/2} = R_Q w_{i+1/2}$ are computed. Eventually, the original conservative variables on the faces are computed from the computed semi-logarithmic semi-conservative face variables as

$$q_{i+1/2} = \begin{bmatrix} e^{[ln(\rho)]_{i+1/2}} \\ e^{[ln(\rho)]_{i+1/2}} u_{i+1/2} \\ e^{[\ln(\rho E)]_{i+1/2}} \end{bmatrix}, \tag{23}$$

for which the density and the total internal energy components always remain positive.

4 RESULTS

4.1 Sod shock tube test case

In order to assess the developed positivity-preserving strategy for WENO, the 1D Sod shock tube test case [11] is presented. Since the solution based on the WENO scheme is positive for this test case, the positivity-preserving property is not important. However, this test case is used to compare the performance of the developed positivity-preserving approach to the other schemes. The left and right initial conditions are $(\rho_L, u_L, p_L) = (1, 0, 1)$, and $(\rho_R, u_R, p_R) = (0.125, 0, 0.1)$, respectively. Here ρ is density, p is pressure, and u is the velocity. The heat capacity ratio is $\gamma = 1.4$.

The simulations are performed using 100 uniform grid cells and with a CFL number of 0.4. At a time t_0, the diaphragm is removed and at $t = 0.2$[s] the exact solution and the simulation results for density are shown in Fig. 1a. The simulations are performed using

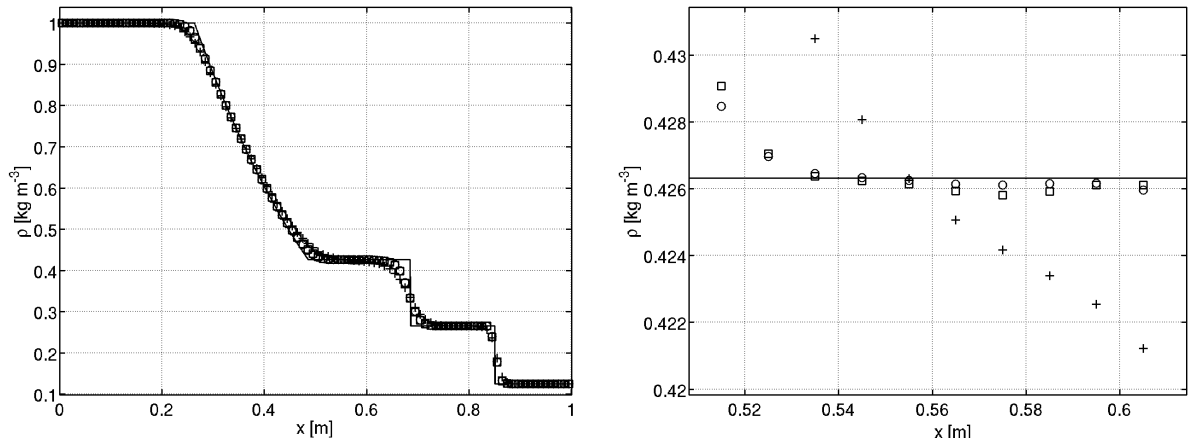

(a) (b)

Figure 1: Density plot for Sod shock tube, with MUSCL (+), characteristic-wise WENO5 (□), and the developed positivity-preserving WENO5 (o), at a time $t = 0.2$[s].

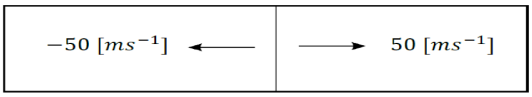

Figure 2: A schematic of the cavitating expanding waves tube.

the characteristic-wise MUSCL, characteristic-wise WENO, and the developed positivity-preserving WENO schemes. Moreover, a 5^{th}-order accurate stencil is used for the WENO scheme which we refer to by WENO5. From Fig. 1b, it is observed that the WENO plots are sharper near the discontinuities compared to the MUSCL plots. Additionally, the positivity-preserving WENO plot has less undershoot compared to the characteristic-wise WENO scheme.

4.2 1D cavitating expanding waves test case

The physical model in combination with the thermodynamic models and the spatial discretization described in previous sections is tested for the 1D cavitating expanding waves [12]. However, the original conditions [12] are modified to suit for the current study purposes. Initially, there is water at rest in a tube with a length of 6[m] (see Fig. 2), and with initial conditions presented in table 1. A diaphragm in the middle of the tube separates the fluids at both sides. At time t_0, the diaphragm is removed and at the same time the fluids on the left and right sides are pulled apart with the speeds of -50[ms^{-1}] and 50[ms^{-1}], respectively. Consequently, cavitation is triggered in the middle of the tube.

The simulations are carried out using 600 uniform grid cells, and for a number of 800 time steps with a time step of $\Delta t = 2 \times 10^{-6}$[s]. The employed discretization schemes are MUSCL, a component/characteristic-wise WENO without the positivity-preserving

p_∞ [10^5Pa]	T_∞ [K]	ρ_∞ [kg m^{-3}]	c_∞ [m s^{-1}]
12.5	303.15	996.13	1539.6

Table 1: Initial conditions for the 1D cavitating expanding waves.

property, and the developed positivity-preserving method for WENO (a 5^{th} order accurate stencil is used for WENO). Due to negative density and/or internal energy problem in characteristic/component-wise WENO scheme, the simulations using these schemes failed. However, using the developed positivity-preserving approach, the simulations were carried out successfully. The results based on the developed positivity-preserving WENO and the MUSCL scheme are shown in Fig. 3.

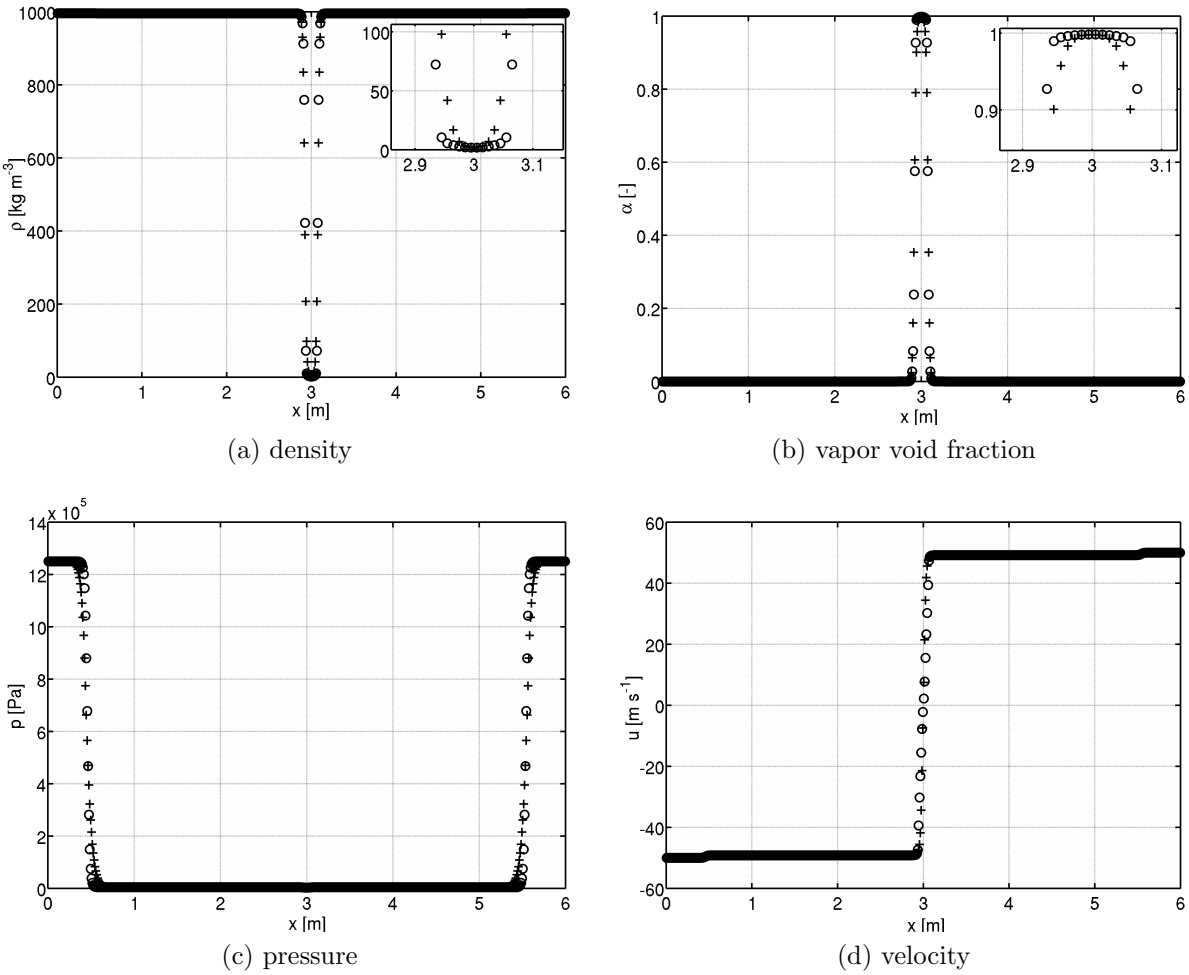

(a) density (b) vapor void fraction

(c) pressure (d) velocity

Figure 3: (continued in the next page)

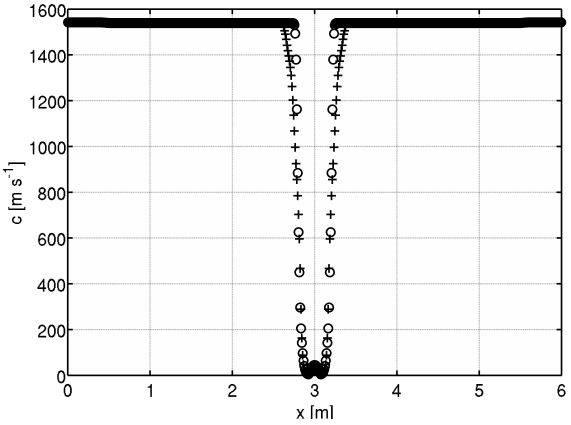

(e) speed of sound

Figure 3: Plots for 1D cavitating expanding waves test case, with developed 5^{th} order accurate positivity-preserving WENO5 (o), and the MUSCL scheme (+).

The solution to this test case corresponds to two rarefaction waves running in opposite directions. In the rarefaction wave, the pressure decreases rapidly to saturation pressure. However, the vapor void fraction only changes in the zones where there is a velocity gradient, and in the rest of the domain it remains equal to zero. This is because that in the regions with zero velocity gradient, despite being in saturation state, there is no mechanism available to provide the latent heat of evaporation in the mixture phase. Here, such mechanism is only available by the kinetic energy reduction in the regions with velocity gradients.

From these figures, it is visible that there are some differences in WENO results compared to the MUSCL results. Fig. 3a and Fig. 3b show that the amount of cavitation in MUSCL results is underestimated compared to the WENO results. A grid dependency study (not included here) showed that the MUSCL results on finer grids converge to the current WENO results. Moreover, Fig. 3c, shows that the WENO solution for pressure is sharper near discontinuities compared to the one obtained using the MUSCL scheme. Finally, Fig. 3e shows a more accurate representation of the speed of sound for WENO results compared to the MUSCL results.

4.3 3D tip vortex cavitation on Arndt's elliptic hydrofoil using the MUSCL scheme

A test case for the unsteady 3D cavitating flow is the flow around an elliptic Arndt's hydrofoil [19, 20] at 7 deg AOA. Since the positivity-preserving WENO scheme has not been extended to multiple dimensions yet, a MUSCL reconstruction scheme is employed. An O-type grid, shown in Fig. 4a, is used consisting of approximately 1860000 cells. Furthermore, a farfield boundary condition is used. The flow is from left to right, and the free-stream conditions are shown in table 2. A cavitation number of $\sigma = 1$ is used in

simulations. The free-stream velocity and pressure are taken with values higher than the standard conditions (keeping the cavitation number constant), to accelerate the cavitation cycles [2]. Moreover, the simulations are carried out using a time step of $\Delta t = 1 \times 10^{-10}$[s]. The small time step is chosen for stability and in order to be able to capture all the physical phenomenon. Additionally, an AUSM+-up for all speeds flux scheme [18] is used in these simulations.

The initial solution for the unsteady cavitating flow is the steady, fully converged

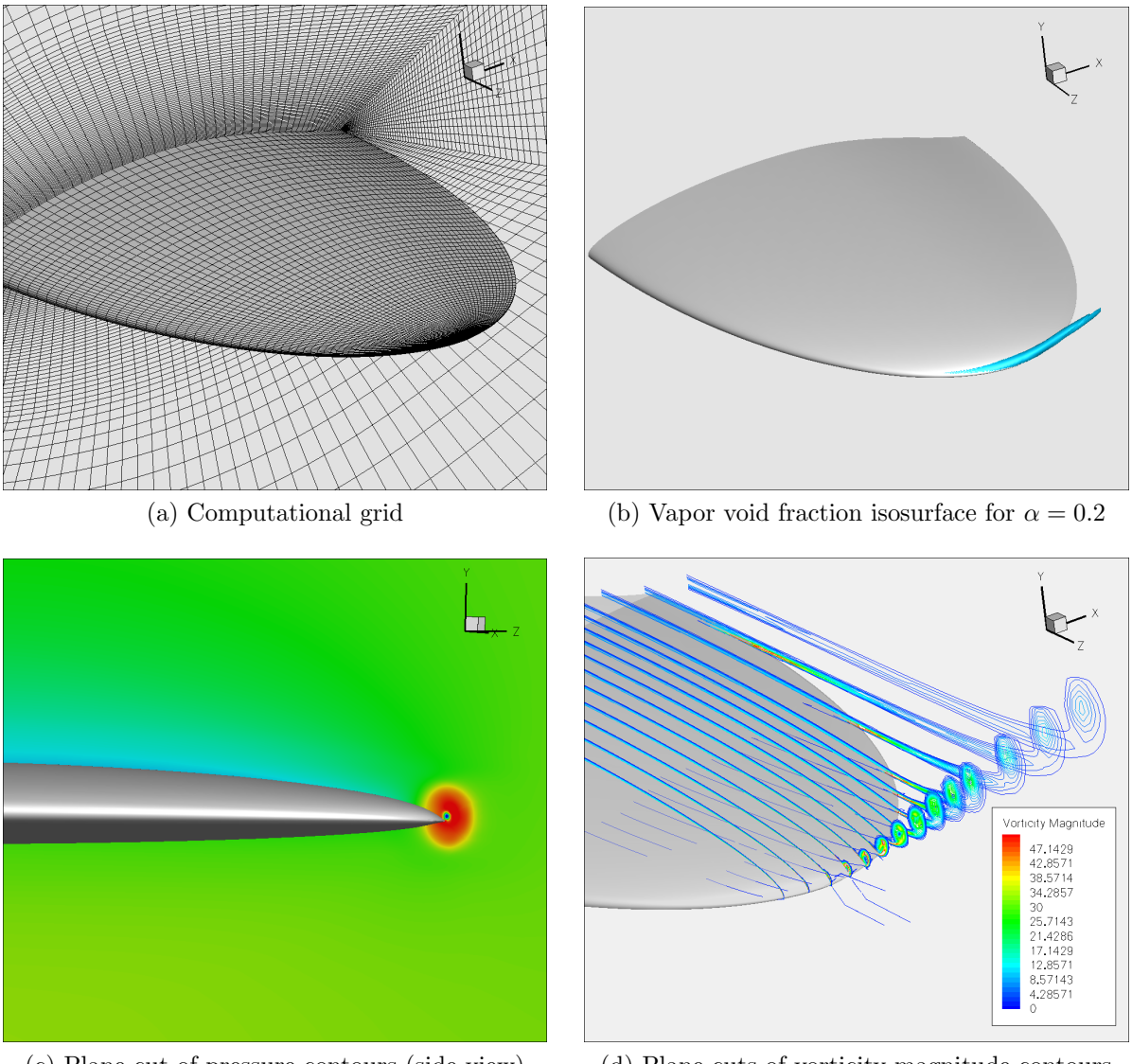

(a) Computational grid

(b) Vapor void fraction isosurface for $\alpha = 0.2$

(c) Plane cut of pressure contours (side view)

(d) Plane cuts of vorticity magnitude contours

Figure 4: Tip vortex cavitation simulations on Arndt's elliptic hydrofoil for $\sigma = 1$, using a computational grid of 1860000 cells, and a MUSCL reconstruction scheme.

U_∞ [m s^{-1}]	p_∞ [10^5Pa]	T_∞ [K]	ρ_∞ [kg m^{-3}]	c_∞ [m s^{-1}]	σ [–]
50	12.5	293	998.7	1540.0	1.0

Table 2: Conditions for the cavitating flow around the Arndt's hydrofoil at 7 deg AOA.

fully wetted flow solution obtained using the modified Tait equation, see section 2. The simulation results are not discussed in detail. Only some specifically chosen plots from different time instances are shown in Fig. 4, which are indicative of the performance of the MUSCL scheme for vortex cavitation simulations. Fig. 4b, depicts the vapor void fraction isosurface for $\alpha = 0.2$. The figure clearly shows the cavotatopm in the tip vortex. In the presented simulations, the cavitating vortex disappears very rapidly, whereas similar experimental studies [20] show that the cavitating vortex should exist until the farfield of the domain. This difference can be explained from the plots in Fig. 4d. This figure is a plot of the vorticity magnitude contours at the tip of the hydrofoil. It is observed that in a short distance downstream of the foil, the vorticity magnitude is decreased with a rather high rate. These plots are indicative of the presence of high artificial dissipation in the simulation results. One solution for this problem is to use a finer grid or to perform adaptive grid refinements. However, this leads to an impractically large number of grid cells. Moreover, the very small time steps (less than nano seconds) in such simulations, would require extremely long computational times.

5 CONCLUSIONS AND FUTURE WORK

- The cavitation equilibrium thermodynamic model [1] following the thermodynamic approach in previous work [4] is employed to model the cavitation.
- The 3D vortex cavitation simulations were performed on the elliptic Arndt's hydrofoil, using the MUSCL reconstruction scheme. The results showed that MUSCL reconstruction schemes are not well-suited for flows involving vortex cavitation.
- A more sophisticated approach based on the Weighted Essentially Non-Oscillatory (WENO) schemes has been considered instead. However, to avoid the problems with negative density or internal energy, the scheme must be positivity-preserving.
- A rather simple non-limiting positivity-preserving strategy for WENO scheme has been developed. Since this scheme does not use any flux/slope limiter functions, it does not introduce any excessive numerical dissipation.
- To assess the method, the Sod shock tube problem [11] and the 1D cavitating expanding waves test case [12] were presented.
- The results showed the robustness of WENO schemes compared to the MUSCL schemes.

- For the cavitating test case simulations using the WENO scheme, the non-positivity-preserving WENO schemes failed. However, the simulations were carried out successfully using the developed positivity-preserving WENO scheme.

- Future work to be carried out is the extension of the developed positivity-preserving scheme to multiple dimensions. Furthermore, the method will be extended to viscous flows using the LES approach for modeling effects of turbulence and apply the method to vortex cavitation.

REFERENCES

[1] Schnerr, G. H., Sezal, I.H., and Schmidt, S.J., Numerical Investigation of Three-Dimensional Cloud Cavitation with Special Emphasis on Collapse induced Shock Dynamics, *Physics of Fluids* (2008), **20**, 4:040703.

[2] Koop, A.H., *Numerical Simulation of Unsteady Three-Dimensional Sheet Cavitation*. University of Twente, the Netherlands, (2009).

[3] Koop, A., and Hoeijmakers, H., Numerical Simulation of Unsteady Three-Dimensional Sheet Cavitation, *Cav2009 Proceedings*, Ann Arbor, Michigan, USA, (2009).

[4] Khatami, F., van der Weide, E., and Hoeijmakers, H., Multi-phase thermodynamic tables for efficient numerical simulation of cavitating flows: A novel approach towards optimized accurate tables, *8th International Conference on Multiphase Flow, ICMF 2013*, Jeju, Korea, (2013).

[5] Leer, van B., Towards the Ultimate Conservative Difference Scheme V. A Second-order Sequel to Godunov's Method, *J. Comput. Phys.*, **32**:101-136, (1979).

[6] Liu, X. D., Osher, S., Chan, T., Weighted essentially non-oscillatory schemes, *J. Comput. Phys.*, **115**:200-212, (1994).

[7] Jiang, G. S., Shu, C. W., Efficient implementation of weighted ENO schemes, *J. Comput. Phys.*, **126**:202-228, (1996).

[8] Zhang, X., Shu, C. W., Maximum-principle-satisfying and Positivity-Preserving High-Order Schemes for Conservation Laws: survey and new developments, *Proc. R. Soc. A Math. Phys. Eng. Sci.*, **467**:2752-2776, (2011).

[9] Xiangyu, Y. H., Adams, N. A., Shu, C. W., Positivity-preserving Method for High-Order Conservative Schemes Solving Compressible Euler Equations, *J. Comput. Phys.*, **242**:169-180, (2013).

[10] Shu, C.-W., Total - Variation - Diminishing time discretizations, *SIAM J. Scientific and Statistical Computing*, **9**:1073-1084, (1988).

[11] Sod, G. A., A Survey of Several Finite Difference Methods for Systems of Nonlinear Hyperbolic Conservation Laws, *J. Comput. Phys*, **27**:1-37, (1978).

[12] Saurel, R., Abgrall, R., A Multiphase Godunov Method for Compressible Multifluid and Multiphase Flows, *J. Comput. Phys*, **150**:425-467, (1999).

[13] Wallis, G. B., *One-dimensional two-phase flow*, McGraw-Hill Book Company, (1969).

[14] Sezal, I. H., *Compressible Dynamics of Cavitating 3-D Multi-Phase Flows*, PhD thesis, Technische Universitt Mnchen, Germany, (2009).

[15] Schmidt, E., *Properties of Water and Steam in SI-Units; 0-800C, 0-1000 bar*, Springer-Verlag. R. Oldenbourg, 4th enlarged printing edition, (1989).

[16] Toro, E. F., Spruce, M., and Speares, W., Restoration of the Contact Surface in the HLL-Riemann Solver, *Shock Waves*, **4**:25-34, (1994).

[17] Liou, M. S., Ten Years in the Making - AUSM-family, *AIAA Paper*, 2521, (1994).

[18] Liou, M. S., A sequel to AUSM, Part II: AUSM+-up for all speeds, *Journal of Computational Physics*, **214**:137-170, (2006).

[19] Maines, B. H., Arndt, R. E. A., Tip Vortex Formation and Cavitation, *Journal of Fluids Engineering*, **119**, 2:413-419, (1997).

[20] Maines, B. H., *Tip Vortex Formation and Cavitation*, PhD thesis, The University of Minnesota, USA, (1995).